Chapter 2

H scattering at Cu(100) [19]

2.1 Introduction

The dynamical interaction of atomic hydrogen with metal surfaces has attracted much attention recently, both theoretically and experimentally. On the one hand side this is due to the practical importance of hydrogen/metal systems in heterogeneous catalysis and for hydrogen storage [20], and on the other side due to the "simplicity" of the H atom which makes it an ideal candidate for fundamental, notably theoretical, investigations. Also, H atoms are involved in most of the few gas-surface reactions of the Eley-Rideal type known so far [21]. It can further be speculated that they also participate in "hot atom" reactions [22] for which the situation is intermediate between pure Eley-Rideal (gas phase atom reacts directly with adsorbed reaction partner), and pure Langmuir-Hinshelwood mechanisms (all reaction partners equilibrated with the surface). In this chapter the H/Cu(100) system will be study in some detail.

When a hydrogen atom hits a metal surface various outcomes are possible. If the substrate is rigid the atom can – in contrast to molecules – only be reflected or enter deep into the bulk, at least if no significant normal to parallel momentum transfer occurs. A real surface, however, is non rigid and both phonons (all substrates) and electron-hole pairs (mostly for

metals), may be excited. Thus, energy can be transferred from the atom to the substrate and this gives rise to the sticking of the atom either as an adsorbed species or as one that is absorbed in subsurface or bulk sites. In principle, electronic excitations at metal surfaces can become as important as or even dominate over the purely mechanical couplings. For example, experiments for H/Al(100) [14] indicate that both relaxation channels contribute about equally to the sticking probability. In contrast, the exact extent of energy transfer due to electron-hole pair creation is still largely unknown for H interacting with various Cu surfaces. Vibrational linewidth measurements for H adsorbed on Cu(111) suggest that a significant contribution of the energy relaxation process is electronic [23]. On the other hand, for H/Cu(110) Brenig *et al.* [24] (using data for H/W) give theoretical evidence that the electron-hole pair mechanism does not significantly contribute to the sticking of H. For systems like He/Cu, similar conclusions had earlier been drawn by Schönhammer and Gunnarson [25]. However, in Ref. [25] it is also argued that for adsorbates with affinity levels close to the metal's Fermi level an electronic sticking mechanism may perhaps dominate. The methods to treat electron-hole pair excitations range from model Hamiltonian / perturbative approaches [25, 26, 27, 28] and non-adiabatic coupling schemes [29], to "molecular dynamics with electronic friction" [10] and other effective-potential methods [30], to electronic wave packet [31], and density matrix models [32].

In this part of the thesis the focus will be solely on phonons, neglecting any possible electronic contributions. This is motivated by the aim to first understand the simpler mechanical coupling problem before addressing the electronic one. A major goal will be the critical assessment of various theoretical methods to treat adsorbate-phonon coupling. The existing methods to describe the coupling of a reaction path/surface to a "bath" of environmental oscillators, are similar in spirit to the methods to treat (bosonic) electron-hole pair environments mentioned above. In general, one may distinguish three major classes of methods: (i) Classical mechanics, (ii) approximate quantum

mechanics, and (iii) mixed quantum-classical schemes.

Among the classical schemes are pure molecular dynamics methods, quasi-classical schemes (which include zero-point corrections), and "system plus bath" approaches such as the (generalized) Langevin [33] or the Fokker-Planck equation [34]. The latter are particularly useful when finite temperature is to be modeled. The classical methods are considered "cheap", while suffering from the lack of quantum effects – clearly a drawback for a typical quantum particle such as hydrogen.

Among the time-dependent, approximate quantum schemes are wave packet methods and reduced density matrix theory. In one class of approximate wave packet methods the dimensionality of the problem is reduced but the "system-bath" coupling treated exactly; examples are the surface oscillator [35] and modified surface oscillator [11] models, in which only single environmental Einstein oscillators are considered. In a second type several or many oscillators are included, with additional approximations for them; an example is the "surrogate Hamiltonian" approach in which the oscillators are idealized as a set of two-level systems [36]. In a third class of approximate wave packet schemes one makes a Hartree-type separation of the system and the oscillators, leading to the Time-Dependent-Self-Consistent-Field (TDSCF) method [37] or multi-configurational variants [38, 39] of it. In open-system density matrix theory the system degrees of freedom evolve under the dissipative action of the bath modes, which are usually assumed to be only weakly coupled to the adsorbate [40]. For scattering of light atoms at heavy atom surfaces this is usually a good idealization, while another commonly used approximation – the Markov one – does often not hold because the phonon bath correlation functions decay typically not quickly enough on the characteristic timescale of the system [40, 41]. The same problem of non-vanishing memory effects occurs also in Langevin theory.

In the following for the H/Cu(100) system among other methods, a mixed quantum-classical scheme in which a H wave packet couples to a classical oscillator will be adopted. In the simplest variant, the "Ehrenfest" or "mean-

field" method, a single configuration of the total wave function is considered (*i.e.*, TDSCF), and then for the bath modes the classical approximation is made (see below) [42]. When a multi-configurational ansatz is used for the wave packet followed by the partially classic treatment, one ends up with various "surface hopping" schemes [43].

Several of the methods just listed will be tested below for the H/Cu(100) system. In the end one wants to treat at least the impinging H atom quantum mechanically and to include substrate atom motion. The interest lies in reflection, adsorption, subsurface absorption and bulk absorption probabilities and how these depend on substrate vibrations. Major difficulties encountered *en route* are (i) the large kinetic energies released when H enters the chemisorption well, and (ii) the long propagation times involved (typically 3 ps). Together with the need to include phonons the "simple" problem of a low-energy gas phase H atom crashing into a movable Cu surface becomes therefore a challenging numerical task – and a challenging testing ground for approximate quantum methods as well.

2.2 Models and potential

2.2.1 Models

From a practical viewpoint the H/Cu(100) system has an infinite number of degrees of freedom even if one only considers the motions of the nuclei, *i.e.*, three spatial coordinates for the hydrogen atom and three additional ones for every copper atom. That is why a reduced-dimensionality model has to be constructed for a numerical simulation of the scattering and sticking of hydrogen on a non rigid copper surface. On the one hand this model should be kept as simple as possible to allow for a systematic comparative study involving different dynamical methods and costly numerical techniques. On the other hand the model must contain the essentials of the physical problem. As a reasonable compromise the "planar model" will be used in this thesis for H/Cu(100).

In the planar model, it is assumed that the H atom and the Cu atoms can move only in two spatial directions x and z, where z is the direction perpendicular to the Cu(100) surface and x the direction along [100] parallel to it [*i.e.*, the line connecting top–hollow–top positions of H on Cu(100)]. All other Cu atoms that are not located in the (x,z) plane are kept at fixed positions in the planar model, but they do contribute to the total interaction potential. In the planar model, periodic boundary conditions are used along x, such that each additional Cu layer contributes one more atom to the elementary cell. The lattice constant in the planar model is $a = 6.831$ a_0. In all cases a six-layer model will be employed. The translation vector along x is shown in Fig. 2.1.

The physical motivation for the planar model is illustrated with reference to Fig. 2.1. The light hydrogen atom can loose only a small amount of kinetic energy during a single collision with a heavy copper atom. So hydrogen has to perform many collisions to loose enough energy and adsorb on the surface. Obviously hydrogen can only remain in the interaction region near the surface for longer times if a so-called normal to parallel momentum transfer occurs.

This means that the momentum gained in z direction while approaching the surface is transferred to momentum along x parallel to the surface. So it is a minimal requirement for a numerical simulation to include surface corrugation, *i.e.*, a one dimensional model (z only) cannot properly describe the sticking of an atom at a surface. The planar model contains two degrees of freedom for the hydrogen motion, where we choose the lateral coordinate parallel to the translation vector of the primitive unit cell of the surface, for which one expects the greatest amount of corrugation. In particular, the following models will be studied based on the planar model:

1. In the "planar rigid surface model" (pRS-2D), none of the Cu atoms is allowed to move and the H atom can only translate in the (x_H,z_H) space – this corresponds to a simple two-mode problem.

2. In the "planar single-surface oscillator model" (p1SO-3D), only the uppermost Cu layer does move and the other five remain rigid. This corresponds to a four-mode problem (x_H,z_H,x_{Cu},z_{Cu}). For perpendicular impact of the H atom, symmetry requires that the motion of Cu along the x direction will not be excited and therefore a three-mode problem arises which will be used as an important benchmark case below. This model is thus very similar to previously used (modified) "surface oscillator" models that employ a single Einstein oscillator only [11].

3. In the "planar N-surface oscillator model" (pNSO-(N+2)D), N Cu atoms are allowed to move in the (x,z)-plane. Below, only results for N=5 will be presented, in which case only the bottom layer remains fixed. For perpendicular impact of H modeled as a plane wave, the problem is (N+2)=7 dimensional, while for non perpendicular impact or a non-plane wave initial wave packet the problem would be (2N+2)=12 dimensional.

Note that in the planar model with periodic boundary conditions all of the (infinitely many) surface atoms in the (x,z)-plane move in phase, correspond-

ing to phonons at their Γ point; phonon dispersion effects will be neglected.

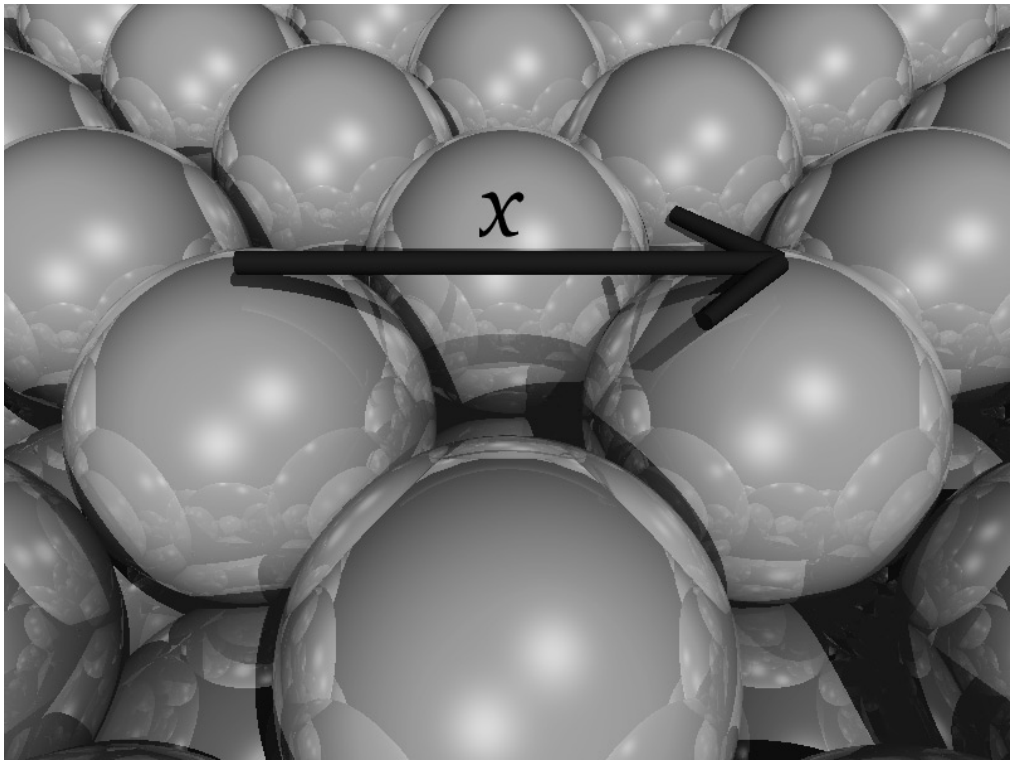

Figure 2.1: The translation vector used along x ([100]) on the Cu(100) surface – planar model. Only atoms in the (x,z) plane are allowed to move, and also H motion is restricted to this plane. The non moving Cu atoms do contribute, however, to the interaction potential.

2.2.2 Potentials

Unfortunately due to the high dimensionality of most models used, one can not rely on *ab initio* quantum chemistry calculations to determine the multi-dimensional potential energy surface. On the other hand it is well known that the interaction potential between hydrogen atoms and metals cannot accurately enough be modeled by a simple empirical pair potential [44]. This has to do with the fact that the metal electrons are delocalized and hence the potential energy contains complicated many body terms. This is particularly true when also the metal atoms are allowed to move and when interactions between the metal atoms have to be accounted for. For example it has been shown that it is not possible to reproduce the experimental elastic constants of metals using a pair potential approach [45], *e.g.*, for a cubic crystal one will always obtain $C_{11} = C_{12}$ and $C_{44} = 0$, which of course is not true for real solids. Here, C_{11}, C_{12}, and C_{44} are the three independent elastic constants for a cubic crystal in Voigt notation.

Therefore, here the so-called EMT potential (Effective-Medium-Theory) is used instead [46]. This is a non-pair potential, similar to the well-known EAM potential (Embedded-Atom-Method) [45], both being semiempirical methods based on density functional theory. Both methods are based on the so-called the Stott-Zaremba corollary [47]. The latter states that the energy (E) of an impurity embedded in a host system is a functional of the unperturbed host electron density ($\rho_h(\underline{r})$) and a function of the position ($\underline{R}$) and the type (atomic number Z) of the impurity atom:

$$E = \mathcal{F}_{Z,\underline{R}}\left[\rho_h(\underline{r})\right] \quad . \tag{2.1}$$

Unlike the Hohenberg-Kohn theorem [48], the Stott-Zaremba theorem cannot be directly used to calculate the self consistent density, because the Stott-Zaremba corollary is not variational. But nevertheless it is a very good starting point to develop semiempirical methods due to the fact that every atom in a solid or a chemical compound can be viewed as an impurity embedded in a host consisting of all other atoms. There are many methods based on the

Stott-Zaremba corollary which are using approximations for the unperturbed host density and the embedding functional. In many cases like for the EAM and EMT potentials the total energy expression is written as a sum of single atom energies. These energies are split into a many-body embedding energy $E_k^e[\rho_k]$ which depends on the embedding electron density ρ_k for atom k, and a pairwise repulsive term $\Phi_{kl}(r_{kl})$ which models the Coulomb repulsion between the ion cores. In the specific case of a Cu surface and one H atom this leads to the following equation [46]:

$$\begin{aligned} V(\underline{r}_H, \{\underline{r}_i\}) = &\sum_i^N E_i^e[\rho_i] + E_H^e[\rho_H] + \sum_{j>i}^N \Phi_{ij}(r_{ij}) \\ &+ \frac{1}{2}\sum_i^N \left[\Phi_{iH}(r_{iH}) + \Phi_{Hi}(r_{Hi})\right] \quad . \end{aligned} \tag{2.2}$$

Here, i is the index of Cu atom i at position $\underline{r}_i$, H is located at $\underline{r}_H$, r_{kl} is the distance between atoms k and l. N denotes the total number of Cu atoms. The many-body "embedding" energy of atom i, $E_i^e[\rho_i]$, is parameterized for a binary system as follows (here shown for one Cu atom i)[46]:

$$E_i^e[\rho_i] = E_o f\left(\lambda_i(s_i - s_{o,i})\right) \tag{2.3}$$

$$f(x) = (1+x)e^{-x} \tag{2.4}$$

$$s_i = s_{o,i} - \frac{1}{\beta\eta_{2,i} + \eta_{1,H} - \eta_{1,j}} \ln\frac{1}{12}\left(\rho_{i,j} + \chi_{i,H}\rho_{i,H}\right) \tag{2.5}$$

$$\rho_{i,k} = \sum_{k\neq i} e^{-\eta_{2,k}\left(r_{ik} - s_{o,k}\right)} \quad . \tag{2.6}$$

In this formulation the embedding energy is a function of s_i, the so-called neutral sphere radius of atom i. The latter depends on the embedding electron densities $\rho_{i,j}$ and $\rho_{i,H}$, where $\rho_{i,j}$ is the density contributed by other Cu atoms and $\rho_{i,H}$ the one from the hydrogen atom, respectively. In the EAM method the density is a superposition of atomic electron densities obtained from Hartree-Fock calculations. In the simpler EMT method used here, the electron densities are written as a sum of exponentials [Eq. (2.6)]. Note that the atomic electron densities are spherically symmetric. $\chi_{i,H}$ is in our case

	Cu	H
$\eta_1/[a_o^{-3}]$	0.0091	0.027
$\eta_2/[a_o^{-1}]$	1.652	2.871
$s_o/[a_o^{-1}]$	2.67	1.2894
$E_o/[E_h]$	-0.129	-0.08713
$\lambda/[a_o^{-1}]$	1.906	4.089
$\kappa/[a_o^{-1}]$	2.74	4.69
$V_o/[E_h]$	0.091	0.00157

Table 2.1: EMT parameters for the H-Cu potential, according to Refs.[49] and [46]

$\eta_{2,H}/\eta_{2,i}$, and $\eta_{1,i}, s_{o,i}, E_{o,i}, \lambda_i$, and $\eta_{2,k}$ are atom specific parameters. The repulsive pair potentials are calculated as follows [again shown for one Cu atom i]:

$$\Phi_{ij}(r_{ij}) = \frac{1}{2}\left(\sum_{j\neq i} V_{ij}(r_{ij}) - 12V_{ij}(\beta s_i)\right) \tag{2.7}$$

$$\Phi_{iH}(r_{iH}) = \chi_{i,H} V_{iH}(r_{iH}) \quad . \tag{2.8}$$

Here,

$$V_{ij}(r) = -V_{o,i} e^{-\kappa_j (r_{ij} - \beta s_{o,j})/\beta} \quad , \tag{2.9}$$

where β is a geometric factor depending on the crystal structure of the specific metal. For an fcc metal (like Cu), $\beta = (16\frac{\pi}{3})^{\frac{1}{3}}/\sqrt{2}$. $V_{o,i}, \kappa_i$ are again atom specific parameters. So for H/Cu the EMT potential has 14 independent parameters. Seven of these are for the isolated Cu system, and have been determined earlier by Jacobsen *et al.* [46] from properties (cohesive energy, bulk moduli, shear modulus), of the bulk Cu crystal. The remaining seven parameters were recently determined by Strömquist *et al.* [49], from slab calculations using density functional theory in the generalized gradient approximation. The calculations done in Ref. [49] were for the H/Cu(111) system and complemented by classical molecular dynamics calculations –

here we assume transferability of the potential parameters to Cu(100). The values of all parameters are given in Table 2.1.

Here no cut off function for the hydrogen atom is applied and for copper only nearest neighbor interactions are taken into account which means the sums for the copper-copper interaction in the potential formula are truncated after the sphere of nearest neighbors. This is done mainly for computational reasons and has virtually no effect on the potential energy as long as the Cu atoms are reasonably close to their equilibrium positions. This is the case for all situations studied in this thesis. A more specific discussion of the EMT potential for H/Cu is given in Refs. [46, 49].

Figure 2.2 shows a contour plot of the EMT potential for the rigid surface, cut through the (x,z)-plane, when a H atom (coordinates x_H,z_H) approaches from the gas phase. In Figure 2.3 we show one dimensional reaction paths on the two dimensional surface of Figure 2.2: One for the approach of H normal towards the on top Cu site [*i.e.*, along the vector (0,0,z_H)], a second one for the approach of H normal towards the hollow site [along ($\frac{1}{2a}$,0,z_H)], and a final one under an angle of 45 degrees (along ($\frac{1}{2a}$,0,$\frac{1}{2a}$)). From both figures the following can be seen: (1) When H approaches Cu(100), a large amount of binding energy is released ($\approx$ 0.1 E_h $\approx$ 2.7eV), which leads to a strong acceleration of the atom before hitting the substrate; (2) the Cu(100) is rather "open"; in particular, there are reaction paths (even for the rigid surface case) for which the absorption of the atom into subsurface and deeper absorption sites is un-activated. The large kinetic energy released during the encounter combined with the openness of the surface has several typical dynamical consequences, which will be outlined below.

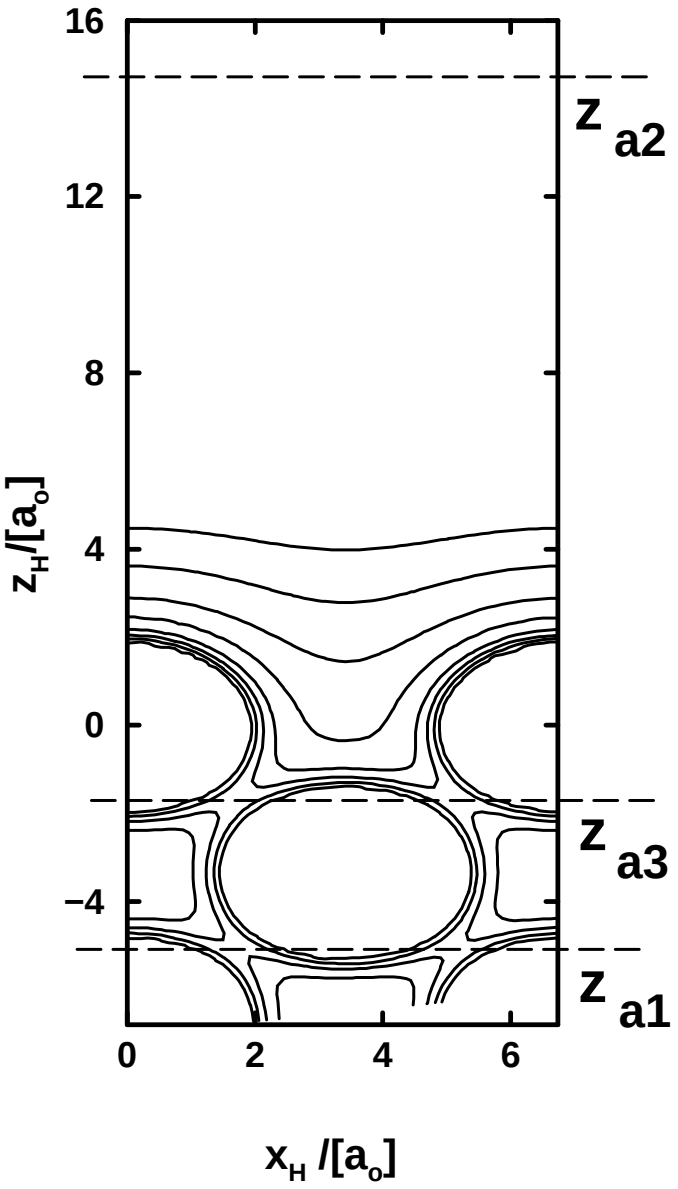

Figure 2.2: 2D contour plot [cut through the (x_H,z_H) plane], of the EMT potential of the H/Cu(100) system. Contours are separated by 0.03 E_h (0.82 eV). The energy-zero corresponds to an H atom far away from the surface. The meaning of the horizontal lines at z_{a1}, z_{a2}, and z_{a3} is explained in the text.

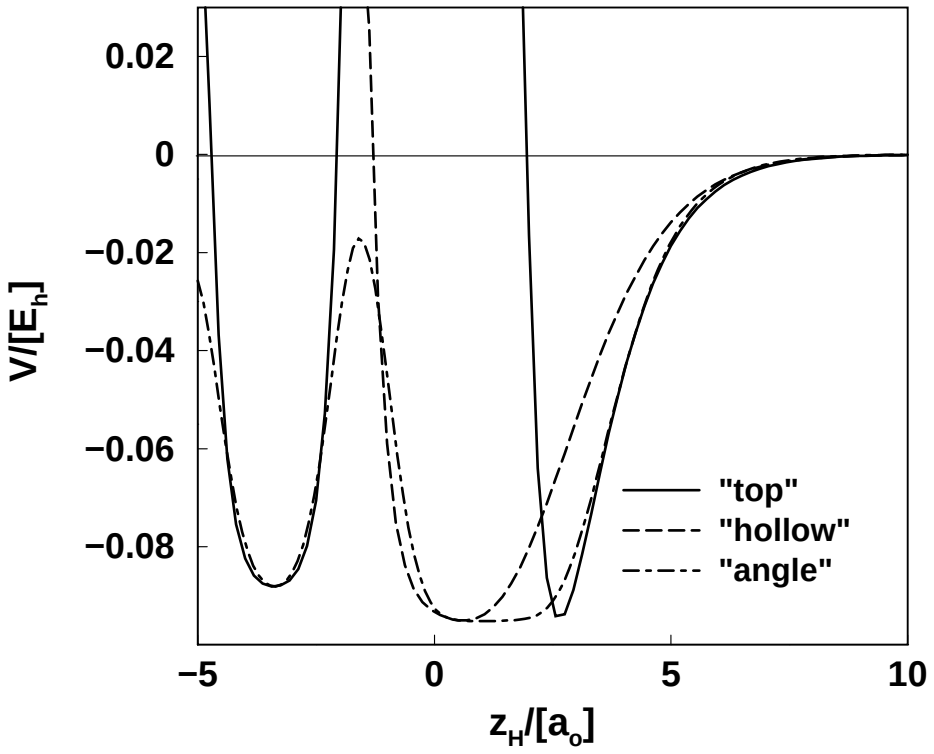

Figure 2.3: 1D "reaction paths" on the 2D potential shown in Fig. 2.2: H approaching Cu on "top" along (0,0,z_H), "hollow" approach along ($\frac{1}{2a}$,0,z_H), and approach under an "angle" of 45 degrees along ($\frac{1}{2a}$,0,$\frac{1}{2a}$).

2.3 Propagation methods

In the following, the (quantum) dynamics of a H atom approaching the surface from the gas phase will be investigated. Four different dynamical methods will be used and compared, mostly for the planar models described in section 2.2.1.

1. A purely quantum mechanical (QM) wave packet method for the models pRS-2D (rigid surface) and p1SO-3D (single-oscillator model);

2. a QCMD method in which a quantum H atom is coupled through Ehrenfest forces to a classical single- or multi-oscillator "bath" of Cu atoms;

3. a single-configuration TDSCF method employing a simplified potential (see below);

4. and classical trajectory calculations (MD).

2.3.1 Quantum mechanical (QM) wave packet methods

(I) pRS-2D model

For the planar rigid surface model pRS-2D a numerical wave packet method is employed to solve the time-dependent Schrödinger equation

$$i\hbar\frac{\partial\psi(x_H,z_H,t)}{\partial t} = \Big[-\frac{\hbar^2}{2m}\left(\frac{\partial^2}{\partial x_H^2}+\frac{\partial^2}{\partial z_H^2}\right) + V\left(x_H,z_H;y_H=0,\{\underline{r}_i=\underline{r}_{i0}\}\right)\Big]\psi(x_H,z_H,t) \quad , \tag{2.10}$$

where $V(x_H,z_H;y_H=0,\{\underline{r}_i=\underline{r}_{i0}\})$ is the EMT potential given in Eq. (2.2), with the copper atoms held fixed at their (relaxed) equilibrium positions $\underline{r}_{i0}$, and m is the hydrogen mass. The Feit-Fleck split operator propagator [50] is employed, a grid with periodic boundaries along x_H, and Fast Fourier Transform (FFT) techniques [50]. The split operator is described in Appendix

A.2 and the FFT in Appendix A.1. Grid and propagation parameters are given in Table 2.2. The initial H wave packet is a Gaussian along z_H (initial position z_0, momentum $\hbar k_{0z}$, width Δz), and a plane wave along x_H, placed well outside the interaction region:

$$\psi(x_H, z_H, t = 0) = N \cdot e^{ik_{0x}x_H}\ e^{-ik_{0z}z_H}\ e^{-(z_H - z_0)^2/(2\Delta z)^2} \quad . \tag{2.11}$$

Here, N is the appropriate normalization factor; all other numerical parameters are given in Table 2.2. In most of the calculations reported below, $k_{0x} = 0$ was taken, *i.e.*, one has a plane wave along x_H and a Gaussian along z_H approaching the surface in normal incidence. Along z_H absorbing boundaries are used to prevent reflection of the (H) wave packet at the grid borders at z_H large and z_H small. Accordingly, in each time step the wave packet is multiplied by "gobbler functions"

$$G_1(z_H) = e^{\gamma_1(z_H - z_{g1})}, \quad z_{g1} > z_H \tag{2.12}$$

$$G_2(z_H) = e^{-\gamma_2(z_H - z_{g2})}, \quad z_{g2} < z_H \tag{2.13}$$

to absorb the parts of the wave packet which have been reflected from the surface and travel towards positive z_H (beyond z_{g2}), and those which enter deep into the bulk (beyond z_{g1}). The bulk absorption and reflection probabilities P_{abs} and P_{ref}, are calculated from the fluxes going through analyzing lines at z_{a1} and z_{a2}, which are situated right in front of the absorber lines (see Figure 2.2). The flux going through the line to analyze the reflected part at $z_H = z_{a2}$, is [51]

$$J(x_H, t; z_{a2}) = \frac{\hbar}{m}\ \mathrm{Im}\left[\psi^*(x_H, z_H, t)\frac{\partial\psi(x_H, z_H, t)}{\partial z_H}\right]|_{z=z_{a2}} \quad , \tag{2.14}$$

and the reflection probability is then

$$P_{ref}(t) = \int_0^a dx_H \int_0^t dt' J(x_H, t'; z_{a2}) \quad . \tag{2.15}$$

Similar expressions hold for the (bulk) absorption probability.

Grid:		
grid start x_H	$x_{H,min}$	0.0 a_0
grid spacing x_H	Δx_H	0.107 a_0
number of grid points x_H	N_{x_H}	64
grid start z_H	$z_{H,min}$	-10.0 a_0
grid spacing z_H	Δz_H	0.117 a_0
number of grid points z_H	N_{z_H}	384
grid start z_{Cu}	$z_{Cu,min}$	-1.23 a_0
grid spacing z_{Cu}	Δz_{Cu}	0.0151 a_0
number of grid points z_{Cu}	$N_{z_{Cu}}$	256
Absorber:		
exponent absorption	γ_1	0.006 a_0^{-1}
absorption line	z_{g1}	-5.55 a_0
exponent reflection	γ_2	0.00034 a_0^{-1}
reflection line	z_{g2}	14.96 a_0
Analysis:		
absorption line	z_{a1}	-5.08 a_0
reflection line	z_{a2}	14.96 a_0
subsurface line	z_{a3}	-1.68 a_0
Initial wave packet:		
center	z_0	17.0 a_0
width	Δz	$\hbar 5/k_{z0}$
Time propagation:		
time step	Δt	4.0 $\hbar/E_h$
propagation time	t_f	125 000 $\hbar/E_h$ (3.024 ps)

Table 2.2: Numerical parameters used in the quantum wave packet calculations for the p1SO-3D model (and, partially, for pRS-2D).

To further analyze the remaining wave packet, the norm of it is calculated for different regions on the grid which are defined through lines (or planes in 3D) at certain values of z_H (see Figure 2.2). Those parts of the wave packet which are located between z_{a1} and z_{a3} correspond to density localized between the first and the second layer of Cu atoms thus contributing to the subsurface absorption probability, $P_{sub}(t)$. Finally, those parts of the wave packet between z_{a3} and z_{a2} are counted as adsorbed, thus contributing to $P_{ads}(t)$. Gobbler parameters and lines, and the analyzing lines are listed in Table 2.2 – see also Figure 2.2.

(II) p1SO-3D model

In the single-oscillator p1SO-3D model the uppermost Cu layer is allowed to move – for normal incidence of H ($k_{0x} = 0$), only along z_{Cu}. In this case the initial wave function was taken to be

$$\Psi(x_H, z_H, z_{Cu}, t = 0) = \psi(x_H, z_H, t = 0) \cdot \phi_0(z_{Cu}) \quad , \tag{2.16}$$

where $\psi(x_H, z_H, t = 0)$ is the 2D wave packet defined in Eq. (2.11), and $\phi_0(z_{Cu})$ is the ground state wave function of the Cu surface oscillator. The latter is obtained from numerically solving a one-mode time-independent Schrödinger equation with an anharmonic potential $V(z_{Cu})$, which arises from the displacement of a Cu atom in the top layer along z and by using the EMT potential (2.2). Also for the third quantum degree of freedom (z_{Cu}), a grid representation is used – see Table 2.2. Again a flux analysis is made right in front of the absorbing boundaries; additionally, the flux is computed in a state-resolved fashion for every of the first 64 eigenfunctions of the Cu oscillator. The hydrogen flux resolved for the surface vibrational state v, $J_v(x_H, t; z_{ai})$ ($i = 1, 2$ for absorption and reflection fluxes), is given by

$$J_v(x_H, t; z_{ai}) = \frac{\hbar}{m} \, \mathrm{Im} \left[C_v^*(x_H, z_H, t) \frac{\partial C_v(x_H, z_H, t)}{\partial z_H} \right] |_{z_H = z_{ai}} \quad , \tag{2.17}$$

where $C_v(x_H, z_H, t) = \langle \phi_v(z_{Cu}) | \Psi(x_H, z_H, z_{Cu}) \rangle_{z_{Cu}}$ is the projection of the 3D wave packet on the Cu eigenfunctions at point (x_H, z_H). The computational

effort for the p1SO-3D model is considerable, because the wave packet has a large kinetic energy and the Cu mass is high, requiring large grids of more than 6×10^6 points. Also, the total propagation time (≈ 3 ps) is long, so that a p1SO-3D wave packet propagation took about one month of CPU time on a medium-sized workstation. This is the reason why as an "exact reference" at present only the planar model is available, and none which is full-dimensional.

Choice of absorbing boundary parameters

An important point is the error due to transmission or reflection at the absorbing boundaries along the z coordinate. This is a well known problem arising by the use of absorbing boundaries in wave packet propagations. Much effort has been devoted to construct reliable absorbers such as gobbler functions or imaginary or complex absorbing potentials (see for example Refs. [52, 53]). Because reflection at or transmission through the absorbing boundary would have serious effects on the results, *i.e.*, the final reflection, adsorption and absorption probabilities, a very careful examination was carried out in the following way for the pRS-2D model to determine the gobbler parameters in Eqs. (2.12) and (2.13).

For the wave packet reflected from the surface the absorber at z_{g2} in Eq. (2.13) has to be suitable for a wide range of momenta along z, reaching from almost zero up to the highest momentum contained in the initial wave packet for the highest kinetic energy ($0.02281 E_h = 0.784$ eV). This is due to the fact that because of the surface corrugation along x any amount of momentum can be transferred form z to x. To test the absorber three different initial wave packets of the form given in Eq. (2.11) were used. The first one has the highest kinetic energy which occurs in the applications in section 2.4, one with a medium kinetic energy and one with a very low kinetic energy. The wave packets were chosen so narrow in momentum space, that almost all components of the wave packet have the same (positive) sign of momentum. In contrast to the scattering calculations of section 2.4 the momentum is not

E_{kin}/eV	$P_{z_{a2}}$	N_r	$t_f/(\hbar/E_h)$
0.0189	0.9988	0.0010	30400
0.272	1.00001	1.9 10^{-9}	34400
0.621	1.0013	8.4 10^{-9}	144000

Table 2.3: Integrated flux $P(z_{a2}) = \int_0^a dx_H \int_0^{t_f} dt' J(x_H, t'; z_{a2})$ of the "absorber test wave packet" with different kinetic energies E_{kin}, going through an analyzing line at $z = z_{a2}$. The absorber parameters γ_2 and z_{g2} in Table 2.2 have been used [see Eq. (2.13)]. Also shown is the "rest norm" N_r remaining unabsorbed, and the total propagation time t_f for each case.

directed towards the surface but away from the surface to the absorber. Also the adsorption and bulk region of the potential energy surface was simply neglected for these tests. After a sufficient propagation time (here 30400 $\frac{\hbar}{E_h}$ for the highest momentum and 144000 $\frac{\hbar}{E_h}$ for the lowest), the integrated flux $P(z_{a2})$ through z_{a2} (see Fig. 2.2) and the norm of the wave function remaining in the interaction region (N_r), were analyzed to estimate the amount of transmission and reflection of the absorber. The results for the three different kinetic energies are shown in Table 2.3. For a "perfect" absorber the integrated flux $P_{z_{a2}}$ should be one and the norm N_r should be zero. The (small) deviation from this ideal values is a measure for the (small) error introduced by the gobbler function in Eq. (2.13).

It is far more complicated to test the absorber placed inside the bulk at z_{g1} which has the task to absorb flux pointing in negative z direction [see Fig. 2.4 and Eq. (2.12)]. In contrast to the region at large z the potential energy varies quickly inside the bulk and hence cannot simply be neglected. Therefore the "backside gobbler" in Eq. (2.12) is tested with an initial wave packet shown in Fig. 2.4. It is a two dimensional Gaussian with the following width and momentum parameters: $k_{x0} = 12.7\ \hbar/a_o$, $k_{0z} = $ -12.7 $\hbar/a_o$, $\Delta x = 0.25\ a_o$, and $\Delta z = 0.25\ a_o$. The total energy is 0.0034 E_h . Due to the large spreading in k-space all relevant momenta are represented. This wave packet

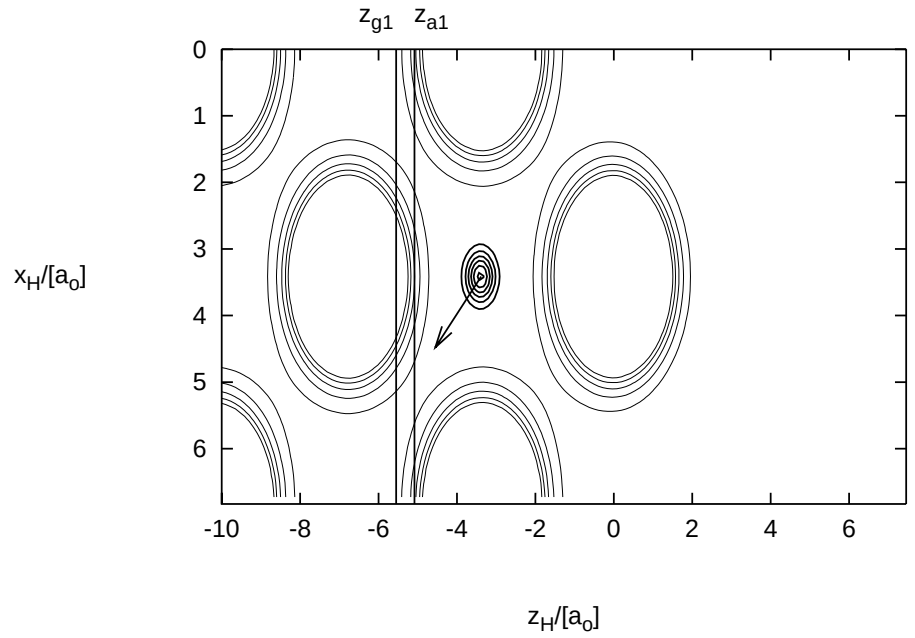

Figure 2.4: A sketch of the initial wave packet used to test the absorber at z_{g1} [see Eq. (2.12)]. The wave packet (thick lines, contours are separated by 0.0062 a_0^{-2}) and the surrounding Cu atoms are shown as contours (thin lines, potential contours ranging from 0.0-0.4 E_h). Also shown is the position of the line at $z = z_{a1}$, where the flux is analyzed. The arrow indicates the direction in which the wave packet is moving initially.

moves initially towards the absorber at z_{g1} under an angle of 45 degrees against the z axis, heading through the gap between the second and third Cu layer. After a propagation time of $t \approx 640\ \frac{\hbar}{E_h}$ the wave packet splits at the diffusion barrier between these two Cu layers (see Fig. 2.5). Finally the main part reaches the lower grid boundary after $t = 800\ \frac{\hbar}{E_h}$. The total integrated flux through z_{a1} is 0.8017 at this time in the absence of an absorber. This means most of the wave packet goes over the barrier and enters the region where the absorber is located. For the time range from 0 to 800 $\frac{\hbar}{E_h}$ the integrated flux through z_{a1} is calculated in the presence of the absorber, and without the absorber. From this one obtains an estimate of the error due to

reflection at the absorbing boundary.

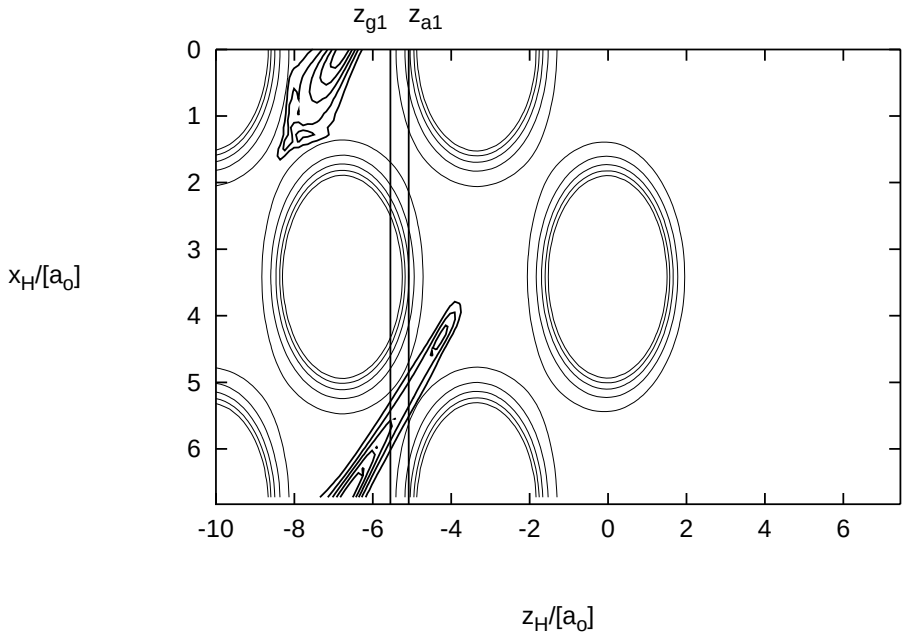

Figure 2.5: A sketch of the same wave packet used in Fig. 2.4 to test the absorber at z_{g1}, after a propagation time of 640 $\frac{\hbar}{E_h}$, without the presence of an absorber. Again shown are the positions z_{a1} and z_{g1} and the surrounding Cu atoms (same contour values as in Fig. 2.4). The contours for the wave packet (thick lines) are separated by 0.0013 a_0^{-2}. One can see that most of the wave packet has moved deeper into the solid and a small part is scattered at the diffusion barrier between the second and third Cu layer, resulting in a splitting of the wave packet. Note the effect of the periodic boundary conditions along x.

The difference between the integrated fluxes through z_{g1} in the absorber "on" and "off" cases, is shown in Fig. 2.6 for three different gobbling parameters γ_1, and as a function of time. Let us first consider the solid line which shows the difference for $\gamma_1 = 0.006 a_o^{-1}$ which will be used in section 2.4. The difference is quite small, as compared to the total flux going through z_{g1} at $t = 800\hbar/E_h$ (≈ 0.8). This demonstrates that the absorber does not

significantly influence the dynamics in the interaction region. Even for a 50 % higher or lower value of γ_1 (dashed and dotted line, respectively) the difference is always lower than $2 \cdot 10^{-5}$.

The long time behavior is tested with the absorber only at z_{g1}. The main part of initial wave packet of Fig. 2.4, which is back scattered between the second and third Cu layer, reaches the z_{a2} line after $\approx 10000 \frac{\hbar}{E_h}$. An estimate for the transmitted part of the wave packet is then given by the difference between the norm of the wave packet between z_{a2} and the upper grid boundary and the integrated flux through z_{a2}, caused by the back scattered part of the wave packet. Here this is $\approx 2.0 \cdot 10^{-5}$. Also no major recrossing of z_{a1} can be observed in this propagation, at least the integrated flux is always rising. This indicates that z_{a1} acts practically as a "line of no return".

In conclusion one can say that the overall error introduced by the absorbers is in the range of a few ‰ only. This error is estimated for the pRS-2D model, but since the light hydrogen atom induces no large amplitude motions of the Cu atoms for the non rigid models, the error due to the absorbers should be in the same order of magnitude also for these models.

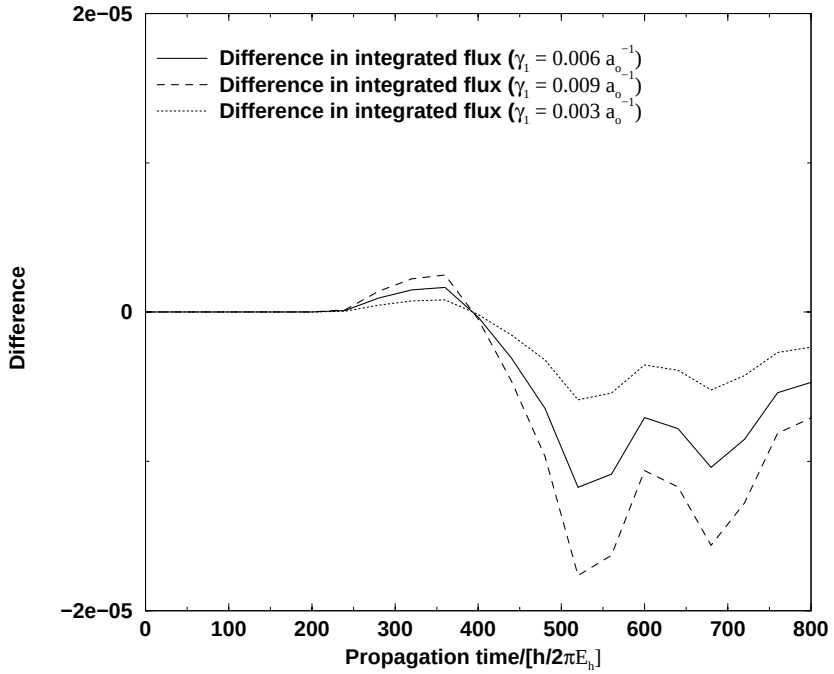

Figure 2.6: Difference in the time-dependent integrated flux through z_{a1} between propagations without and with an absorber. The gobbler parameter in Eq. (2.12) was $\gamma_1 = 0.006\ a_o^{-1}$ (solid line, used in the final propagations of section 2.4), $\gamma_1 = 0.009\ a_o^{-1}$ (dashed line), and $\gamma_1 = 0.003\ a_o^{-1}$ (dotted line).

2.3.2 The mixed Quantum-Classical-Molecular-Dynamics (QCMD) method

Apart from the reduced-dimensionality treatment, the quantum dynamical methods of section 2.3.1 are "exact" for the given potential. In the present section additional approximations will be made to treat the motion of the Cu substrate. In particular, the heavy Cu atoms will be treated classically while the quantum nature of the light H atom will still be retained. There are two basic approximations leading to the QCMD method: First, a single-configuration product ansatz for the total wave function is made,

$$\Psi(\underline{r}_H, \{\underline{r}_i\}, t) = \psi(\underline{r}_H, t) \cdot \Phi(\{\underline{r}_i\}, t) \quad , \tag{2.18}$$

and second, the slow modes (Cu vibrations) are treated classically. This leads to the well-known coupled equations [54]

$$i\hbar \frac{\partial \psi(\underline{r}_H)}{\partial t} = \left[-\frac{\hbar^2}{2m} \underline{\nabla}^2_{\underline{r}_H} + V(\underline{r}_H, \{\underline{r}_i(t)\}) \right] \psi(\underline{r}_H, t) \tag{2.19}$$

$$M \frac{\partial^2 \underline{r}_i}{\partial t^2} = -\langle \psi | \underline{\nabla}_{\underline{r}_i} V | \psi \rangle_{\underline{r}_H} \quad , \tag{2.20}$$

where M is the mass of a Cu atom. According to Eq. (2.19), the motion of the H wave packet depends parametrically on the actual, classical positions of $\{\underline{r}_i(t)\}$ of the Cu atoms. The Cu atoms themselves are coupled to the quantum system by the *Ehrenfest force* $-\langle \psi | \underline{\nabla}_{\underline{r}_i} V | \psi \rangle_{\underline{r}_H}$, which is the negative of the (average) expectation value of the derivative of the potential along the Cu coordinates.

The above equations of motion have been integrated for two different potential functions. In the "exact" QCMD method, the full anharmonic many-body EMT potential V given by Eq. (2.2) is used. In a "linearized" QCMD method, the EMT potential is Taylor expanded in the Cu displacement coordinates $\underline{s}_i = \underline{r}_i - \underline{r}_{i0}$, around the substrate equilibrium positions $\{\underline{s}_i\} = 0$, and truncated after second order, giving an approximate potential

$\overline{V}$:

$$\begin{aligned}\overline{V}(\underline{r}_H, \{\underline{s}_i\}) = \quad & V(\underline{r}_H, \{\underline{s}_i = 0\}) - \sum_{i=1}^{N} \sum_{\alpha=x,y,z} f_{i\alpha}(\underline{r}_H) \cdot s_{i\alpha} + \\ & \frac{1}{2} \sum_{i,j}^{N} \sum_{\alpha,\beta} k_{i\alpha,j\beta}\ s_{i\alpha}\ s_{j\beta} \quad .\end{aligned} \tag{2.21}$$

Here N is the number of Cu atoms considered and $f_{i\alpha}(\underline{r}_H)$ is the force acting along direction α $(= x, y, z)$ on the H atom at position $\underline{r}_H$, due to the displacement $s_{i\alpha}$ of Cu atom i along α:

$$f_{i\alpha}(\underline{r}_H) = -\frac{\partial V}{\partial s_{i\alpha}}|_{\{\underline{s}_k=0\}} \quad . \tag{2.22}$$

It is further assumed that the dependence of the force constant matrix elements $k_{i\alpha,j\beta}$ on $\underline{r}_H$ can be neglected, and that they are given by the second derivative of the potential at $z_H \to \infty$:

$$k_{i\alpha,j\beta} = \frac{\partial^2 V}{\partial s_{i\alpha} \partial s_{j\beta}}|_{\{\underline{s}_k=0\};z_H\to\infty} \quad . \tag{2.23}$$

This latter assumption is additional to the truncation of the expansion of the potential, and means simply that one neglects any frequency shifts in the Cu crystal due to the approaching H atom. The numerical effort to solve the QCMD equations (2.19) and (2.20) is reduced considerably when the approximate potential $\overline{V}$ is used rather than the exact EMT potential (2.2); for the p1SO-3D model, for example, one saves about a factor of 40.

A rather difficult point for numerical applications of this "linearized" potential given by Eq. (2.21) are very high potential gradients which appear in the repulsive regions near the ion cores of the copper atoms. In these highly repulsive regions, a very small norm of the wave packet is built up during a long time propagation, due to the limited numerical precision one can reach by using a computer. (In the propagation presented in this thesis always DOUBLE PRECISION floating point numbers were used following the IEEE standardization [55].) This clearly reduces the long time stability of a propagation and can lead to very large amplitude motions of the Cu atoms,

which have no physical meaning and are only caused by numerical limitations. To tackle this problem a force respectively energy cut off is introduced in order to allow propagations over the long times (≈ 3 ps) needed for the H/Cu system. The repulsive gradients are cut off at a value equal to ≈ 2.5 times the maximal attractive gradient of the potential energy surface. Test calculations showed that the long time results were almost identical for factors in the range from 0.8 up to 5. Only above a factor of five the propagation became unstable. The introduction of a cut off for the repulsive gradients corresponds implicitly to the cutting off of prohibitively high potential energies.

The QCMD equations are solved by using the so-called PICKABACK propagator [56]. Consider a problem were one quantum degree of freedom (q, $\hat{p}$) is coupled to a single classical one (Q, P), then the symplectic PICKABACK performs the propagation from time t to $t + \Delta t$ as follows:

$$Q(t + \frac{\Delta t}{2}) = Q(t) + \frac{P(t)}{M} \frac{\Delta t}{2} \tag{2.24}$$

$$\psi(q, t + \frac{\Delta t}{2}) = e^{-i \frac{\hat{p}^2}{2m} \frac{\Delta t}{2\hbar}} \psi(q, t) \tag{2.25}$$

$$\begin{aligned} P(t + \Delta t) =& P(t) \\ & - \Delta t \left\langle \psi(q, t + \frac{\Delta t}{2}) \left| \frac{\partial V(q, Q)}{\partial Q}|_{Q(t+\frac{\Delta t}{2})} \right| \psi(q, t + \frac{\Delta t}{2}) \right\rangle_q \end{aligned} \tag{2.26}$$

$$\psi(q, t + \Delta t) = e^{-i \frac{\hat{p}^2}{2m} \frac{\Delta t}{2}} \; e^{-iV(q, Q(t+\frac{\Delta t}{2})) \frac{\Delta t}{\hbar}} \; \psi(q, t + \frac{\Delta t}{2}) \tag{2.27}$$

$$Q(t + \Delta t) = Q(t + \frac{\Delta t}{2}) + \frac{P(t)}{M} \frac{\Delta t}{2} \tag{2.28}$$

A very useful consequence of the symplecticity is that the PICKABACK propagator conserves the total energy in the long time average. The split operator (SPO) described in Appendix A.2 has the same property.

2.3.3 The Time-Dependent-Self-Consistent-Field method (TDSCF)

The TDSCF method is another approximate method to treat the dynamics of a system. Unlike the QCMD method both the H atom and the Cu substrate

are treated fully quantum mechanically. For the TDSCF propagation the same single-configuration approximation as in (2.18) is used [37]. When further the substrate wave function is written as

$$\Phi(\{\underline{s}_i\}) = \prod_{i=1}^{3N} \phi(s_i) \quad , \tag{2.29}$$

one obtains for a M dimensional "system" wave packet an M dimensional adsorbate Schrödinger equation which is coupled to 3N one dimensional, uncoupled Schrödinger equations for the bath oscillators. [To simplify the notation in Eq. (2.29) and below, now a single index i is used rather than two indices i and α (atom and spatial component), for the components of the displacement vectors.] If further the surface oscillators are harmonic and if the coupling between system and reservoir is linear in the bath displacement coordinates, it has been shown [37] that the bath can be integrated out analytically. In this case one obtains a single, non-linear M dimensional Schrödinger equation given by [37]:

$$i\hbar \frac{\partial}{\partial t}\psi(\underline{r}_H, t) = \left(\hat{H}_0 - \sum_{i=1}^{3N} \langle \overline{s}_i \rangle \ \overline{f}_i(\underline{r}_H) \right) \psi(\underline{r}_H, t) \quad . \tag{2.30}$$

The position expectation value of oscillator i is in this special case

$$\begin{aligned} \langle \overline{s}_i \rangle =& \langle \overline{s}_i \rangle_0 \ \cos(\omega_i t) + \langle \hat{\overline{p}}_i \rangle_0 \frac{\sin(\omega_i t)}{M\omega_i} + \\ & \frac{1}{M\omega_i} \int_0^t dt' \sin\left[\omega_i (t - t')\right] \langle \psi(t') | \overline{f}_i | \psi(t') \rangle_{\underline{r}_H} \quad , \end{aligned} \tag{2.31}$$

where the $\langle \overline{s}_i \rangle_0$ and $\langle \hat{\overline{p}}_i \rangle_0$ are initial positions and momenta. Eqs. (2.30) and (2.31) can be used for this problem, when the following adjustments are made: (1) The approximate potential $\overline{V}$ (2.21) is used rather than the full EMT potential; (2) the unperturbed system Hamiltonian is $\hat{H}_0 \equiv \hat{T} + V(\underline{r}_H, \{\underline{s}_i = 0\})$, containing only the H-rigid surface interaction potential; (3) the force constant matrix $\mathbf{k}$ in Eq. (2.21) is diagonalized to give the $3N$ normal modes $\{\overline{s}_i\}$ and substrate normal frequencies $\{\omega_i\}$, and (4) the $3N$ force components $\{\overline{f}_i\}$ are derived from the "Cartesian" forces f_i in Eq. (2.22). Hence the

non-linear Schrödinger equation (2.30), sometimes also called a "quantum generalized Langevin equation" [37, 57], derives from the truncated potential (2.21) plus the transformation to normal coordinates. Equation (2.30) is integrated with the SPO propagator (see Appendix A.2) and equation (2.31) by a simple Euler method (Appendix A.3). Note that the TDSCF equations above contain "memory", *i.e.*, no Markov approximation is made.

The normal modes and their frequencies obtained by diagonalizing the force constant matrix $\mathbf{k}$ for the p5SO-12D model are given in Fig. 2.7. In this model, the 5 Cu atoms in the different layers can move in (x, z) direction, hence we obtain 10 normal modes. Because the rigid Cu atoms also contribute to the force constants and introduce fixed boundary conditions, there are no translations or rotations. The normal modes are calculated for hydrogen infinitely far away from the surface. Note that for a normal incidence of the H atom only the "vertical" modes can be excited due to the symmetry of the system.

None of the "surface" modes shown in Fig. 2.7 has an energy larger than about 150 cm^{-1}, corresponding to a Debye temperature of about 220 K. For comparison, the experimental Debye temperatures of Cu are ≈ 315 K for the bulk crystal, and ≈ 170 K for the surface [10]. On the other hand, H atoms adsorbed on a Cu surface have (depending on the adsorption site), typical vibrational frequencies between 1000 and 2000 cm^{-1} and above [49]. As a result of this frequency mismatch multi-phonon excitation has to be present to make a substantial energy transfer from the adsorbate to the substrate and hence sticking possible. In fact this prediction is confirmed by the numerical simulations below.

$\hbar\omega_{10} = 151.1$ cm^{-1} $\hbar\omega_9 = 150.2$ cm^{-1}

$\hbar\omega_8 = 141.4$ cm^{-1} $\hbar\omega_7 = 139.2$ cm^{-1}

$\hbar\omega_6 = 123.9$ cm^{-1} $\hbar\omega_5 = 121.8$ cm^{-1}

$\hbar\omega_4 = 102.5$ cm^{-1} $\hbar\omega_3 = 102.4$ cm^{-1}

$\hbar\omega_2 = 88.35$ cm^{-1} $\hbar\omega_1 = 82.99$ cm^{-1}

Figure 2.7: Calculated normal modes for the multiple-oscillator p5SO-7D model and their energies. In those calculations with $k_{0x} = 0$, only the five "vertical" modes 2,3,5,7, and 9 have to be considered, resulting in the p5SO-7D model.

2.3.4 Classical Molecular Dynamics (MD) calculations

As a fourth and final method the H/Cu dynamics has been treated fully classically. For the classical equations of motion a fourth-order Runge Kutta integrator is used [58] (see Appendix A.4). Again, all Cu atoms are initially in their equilibrium positions. In order to compare the results to the quantum and mixed quantum-classical propagations many trajectories were run and the outcome weighted over a Wigner distribution [59] of the initial wave packet. The periodic boundary conditions are the same as for the quantum grid. The individual trajectories are classified as follows:

- H is counted as *adsorbed* or *subsurface absorbed*, if its total energy (kinetic plus potential) is below -0.07 E_h in average over the last 4000 time steps.

- If H passes the flux lines at z_{a1} and z_{a2} used for analysis in the quantum mechanical calculation (see Figure 2.2), it is counted as *absorbed* or *reflected*, respectively.

- When H is still in the interaction region after 3 ps but has an energy of more than -0.07 E_h, it is classified as "uncertain" ("UC") – but it is reasonable to assume that most of these trajectories will finally lead to adsorption, or subsurface absorption.

When the initial momentum along x is set to zero for the quantum calculations [$k_{0x} = 0$ in Eq. (2.11)], to sample the classical initial conditions only the position in x_H is varied, and the momentum along z_H. Due to the symmetry of the unit cell those trajectories with $x_H(t = 0) = x_a$ give the same results as those with $x(t = 0) = a - x_a$. For a given initial momentum in z_H, of p_{iz}, the statistical weight for all these trajectories differing in $x_H(t = 0)$ is the same because $\psi(t = 0)$ is chosen as a plane wave along x_H. So only the statistical weight for different p_{iz} needs to be calculated as

$$w_{p_{iz}} = N \cdot e^{-(p_{iz} - \hbar k_{0z})^2/(2\Delta p_z^2)} \quad . \tag{2.32}$$

Here, $\hbar k_{0z}$ is the mean momentum defined in (2.11), Δp_z the momentum uncertainty from the corresponding quantum calculation, and N an appropriate factor to normalize the sum of all probabilities to 1. The trajectories are evenly sampled from $x_H = 0$ to $x_H = a/2$ and $p_{iz} = \hbar k_{0z} - 4.5\Delta p_z$ to $p_{iz} = \hbar k_{0z} + 4.5\Delta p_z$, using for both the position and the momentum 101 equidistant values. This corresponds to about 10^4 trajectories for every incident energy.

2.3.5 Reliability of the propagators

Due to the absorbing boundaries the energy conservation after each time step cannot be used as a criterion to determine the right time step in the (semi-) quantum methods. Therefore a "worst case" scenario is set up to examine the energy conservation on a short timescale, where the absorbers have still no effect on the norm of the wave packet. (Due to their symplectic nature the SPO and PICKABACK propagators will conserve the energy in the long time average in any case.)

The test wave packet for this "worst case scenario" is shown in Fig. 2.8. It is a 2D Gaussian along x and z placed in the hollow site adsorption minimum. A large initial momentum along z was chosen ($\hbar k_{0z} = -20.2\ \sqrt{E_h\ 2\ m_e}$). This corresponds to a total energy of $\approx 0.02\ E_h$, which is in the order of the highest incident energy used in this work. The wave packet is propagated for 1000 $\frac{\hbar}{E_h}$ with different time step lengths. After this time the wave packet has not yet reached the grid borders along z. No gobbler is applied during the propagation. The pRS-2D model is used for the split operator and the p5SO-12D model for the PICKABACK propagator, respectively.

Fig. 2.9 gives the total energy of the wave packet [SPO (a)] and the total energy of the quantum plus the classical system [PICKABACK (b)] for different time steps. The large variation in total energy at early times is due to the first collision of the H atom with Cu and caused by numerical errors. After that the initial energy is retrieved, which is an intrinsic property of symplectic propagators. According to Fig 2.9 a time step length of 4 $\frac{\hbar}{E_h}$ is

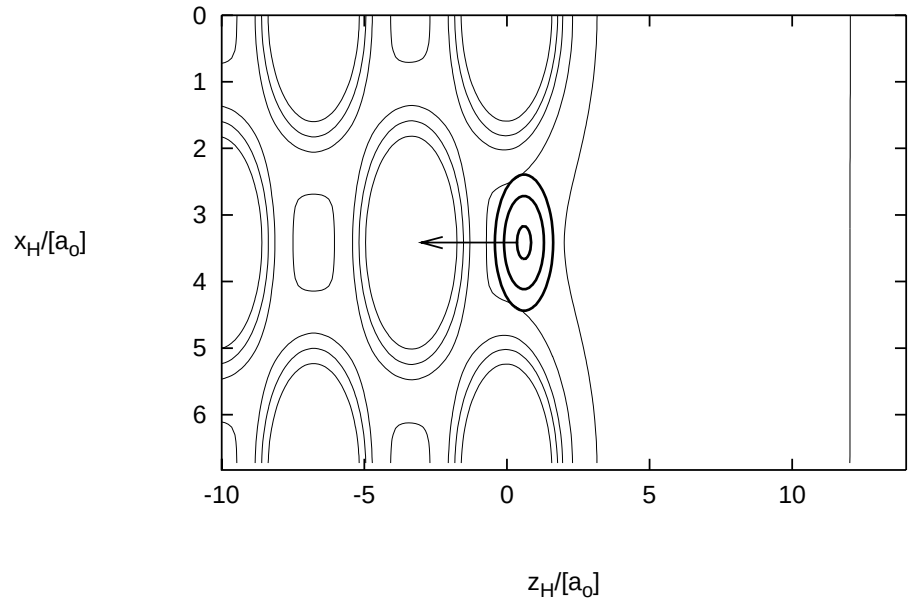

Figure 2.8: A sketch of the initial wave packet used to test the PICK-ABACK and and split operator propagators (the thick lines are a contour of the hydrogen density at 0.0013, 0.0038, 0.0088 a_0^{-2}). The surrounding potential energy surface is indicated by the thin contour lines (contours at -0.08,-0.00001,0.1,0.3 E_h). The wave packet moves directly towards the second layer Cu atom (arrow).

appropriate in both cases (a) and (b). The grid spacing seems to be small enough too, because the error virtually vanishes for very small time steps in the SPO case. This means that the whole range of relevant kinetic energies can be represented in momentum space.

For the TDSCF calculations one can use the fact that this method is formally equivalent to the QCMD method when the linearized potential is used (see below). So by comparing both methods it could be verified that for the TDSCF a time step of 4 $\frac{\hbar}{E_h}$ is also appropriate. Finally for the MD a simple check of the total energy during each trajectory calculation is performed. This indicates that here even slightly larger time step could be

used, but for convenience the same time step of $\Delta t = 4\hbar/E_h$ was used in all propagations.

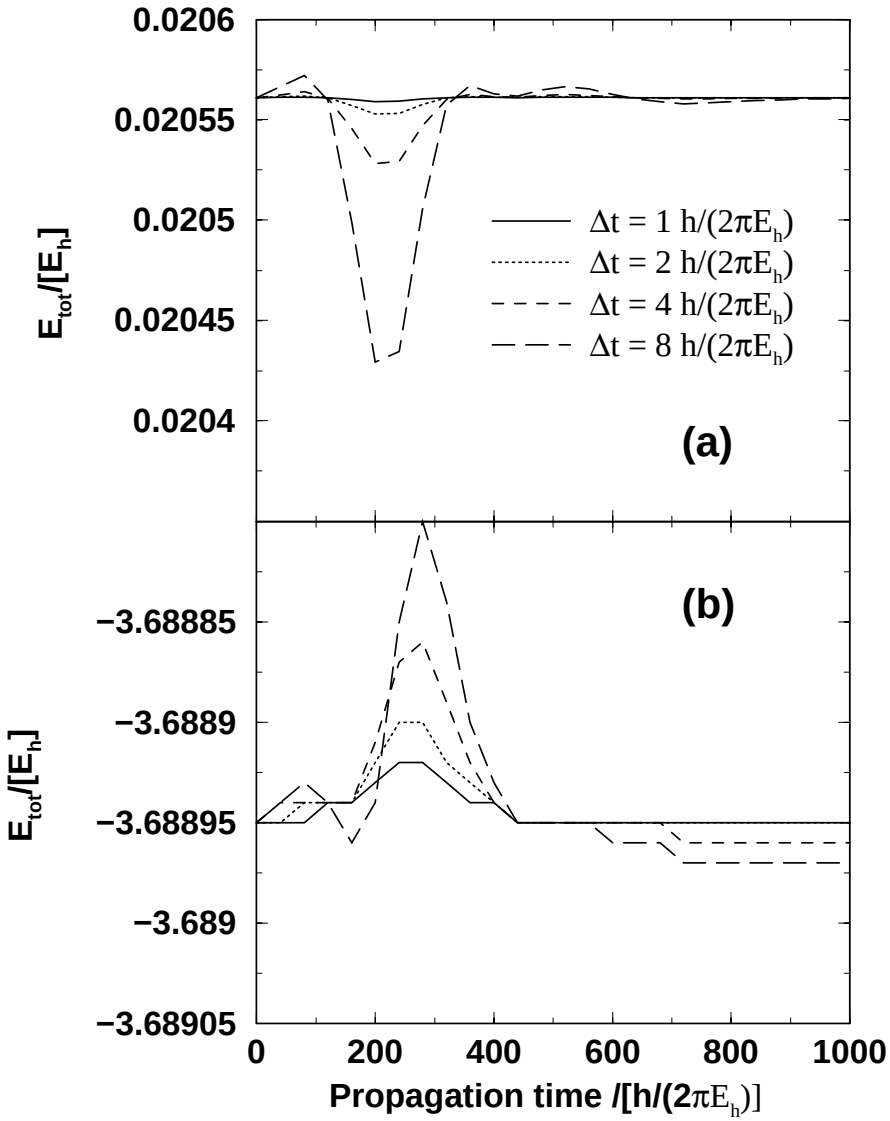

Figure 2.9: Total energy during the propagation of the initial wave packet shown in Fig. 2.8, for the split operator (a) and PICKABACK (b) propagation. Different time steps Δt are used. Note that for the PICKABACK case the potential and kinetic energy of all non rigid Cu atoms is included in the total energy expression, thus leading to a much lower energy.

2.4 Results and discussion

2.4.1 Rigid surface and single oscillator calculations

In a first step, the scattering of H atoms at a Cu(100) surface using the above-mentioned rigid surface (pRS-2D) and single-oscillator (p1SO-3D) models will be described. The hydrogens approach in normal incidence, and four different initial kinetic energies $E_{kin}(0)$ between 0.0075 E_h (0.20 eV) and 0.0228 E_h (0.62 eV) are considered.

I. Rigid surface

Let us consider the rigid surface case first. As outlined above, for rigid surfaces the only possible outcomes of the scattering process are reflection with probability P_{ref}, and bulk absorption with probability P_{abs}. These quantities are time-dependent and become effectively constant in the long time limit, *i.e.*, for $t > t_f$. In Table 2.4, $P_{ref}(t_f)$ and $P_{abs}(t_f)$ are tabulated for various $E_{kin}(0)$, as obtained with the quantum mechanical (QM) wave packet method.

$E_{kin}(0)/[E_h]$	$P_{abs}(t_f)$	$P_{ref}(t_f)$	$1 - P_{abs}(t_f) - P_{ref}(t_f)$	$t_f/[\hbar/E_h]$
0.00745	0.1619	0.8377	$4.5\ 10^{-4}$	103 600
0.01164	0.1800	0.8198	$3.0\ 10^{-4}$	96 800
0.01675	0.1473	0.8523	$4.6\ 10^{-4}$	68 600
0.02281	0.1236	0.8760	$4.9\ 10^{-4}$	60 000

Table 2.4: Rigid surface model pRS-2D: Final bulk absorption and reflection probabilities $P_{abs}(t_f)$ and $P_{ref}(t_f)$ for various initial kinetic energies $E_{kin}(0)$ of the H wave packet; also given are the final propagation times, and the "rest norms" $1 - P_{abs} - P_{ref}$, the latter being the same order of magnitude as the estimated numerical error (see Table 2.3).

One first recognizes that t_f has to be chosen the longer the slower the projectiles, roughly according to $t_f \propto 1/\sqrt{E_{kin}(0)}$. For the lowest kinetic energy the final propagation time t_f is 103600 $\hbar/E_h$, or ca. 2.5 ps. One further notes that reflection dominates over absorption in all cases, but the amount of absorption is always larger than 0.12 and therefore clearly non-negligible. This is a consequence of the open structure of the Cu(100) surface.

From the table one also notes that (apart from a small rise at lowest energies), the bulk absorption probability decreases with increasing kinetic energy. One could attribute this behavior to "steering" of the H wave packet: At higher $E_{kin}(0)$, the wave packet has not enough time to be effectively steered along the low- or no-activation energy paths leading to bulk absorption. At higher energies than those considered here, one would expect that the bulk absorption energy will go up again because then enough energy is available to overcome even higher barriers. Such a "first down, then up" curve is typical also for other gas-surface systems whose dynamics involves unactivated reaction paths on a multi-dimensional potential energy surface [6, 60].

II. Single-oscillator case: "Exact" QM calculations

The QM absorption and reflection probabilities for the rigid surface pRS-2D model are shown in Fig. 2.10 in a time resolved fashion, for the lowest kinetic energy studied, $E_{kin}(0) = 0.00745$ E_h, now for times of up to 125000 $\hbar/E_h$ (3.024 ps). It can clearly be seen that the process takes not longer than 1-2 ps to be complete.

The situation changes dramatically when a single Einstein oscillator (p1SO-3D model) is quantum mechanically (QM) coupled to the H wave packet. In this case the absorption probability in the long time limit increases (to about 0.22 after 3 ps), relative to the rigid surface for which $P_{abs}(3ps) \approx 0.16$. At the same time the reflection probability is reduced from $P_{ref}(3ps) = 0.84$ (rigid surface) to $P_{ref}(3ps) = 0.70$ (non rigid surface). Also, in contrast to the rigid surface case, one has now the possibility that

the H atom sticks on the surface either in adsorption [P_{ads}(3ps) ≈ 0.06], or subsurface absorption sites [P_{sub}(3ps) ≈ 0.01]. Exact final-time probabilities are given in Table 2.5. Hence, the tendency for "sticking", *i.e.* to either absorb or adsorb H atoms increases when the Cu(100) is allowed to move. The now favored bulk absorption is due to the opening up of more low- or no-activation energy paths when the Cu atoms retreat from the incoming H atom. The non-zero probability to stick at surface or near-surface sites is due to the energy loss from the H wave packet to the non rigid surface, which slows down and finally traps the H atom. This energy transfer process can be more clearly visualized by looking at the surface-oscillator state resolved reaction probabilities $P_{v,ref}$ and $P_{v,abs}$, derived from the state-resolved fluxes (2.17), as shown in Fig. 2.11.

Method	P_{abs}	P_{ref}	P_{ads}	P_{sub}
QM	0.2245	0.7036	0.0592	0.01273
QCMD(V)	0.1826	0.8170	0.00035	1.7810^{-5}
QCMD($\overline{V}$)	0.1904	0.8035	0.0057	0.00045
TDSCF	0.1907	0.8031	0.0057	0.00043
	P_{abs}	P_{ref}	$P_{ads} + P_{sub}$	UC
MD	0.2635	0.6414	0.01300	0.08113

Table 2.5: Single-oscillator p1SO-3D model: Comparison of different propagation methods. Given are the final reaction probabilities ($t_f = 1250000$ $\hbar/E_h$), for an initial kinetic energy of the H wave packet of $E_{kin}(0) = 0.00745$ E_h. The abbreviations are explained in the text. "UC" means "uncertain".

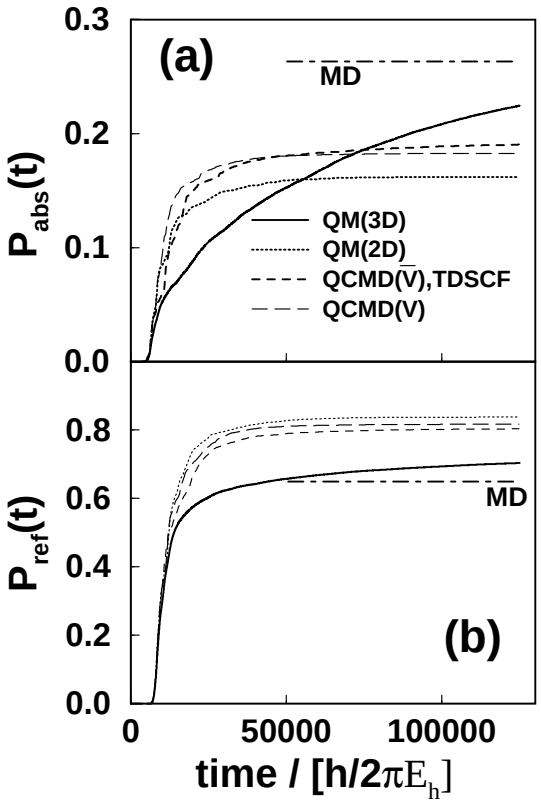

Figure 2.10: Rigid surface (pRS-2D) and single-oscillator (p1SO-3D) models for H/Cu(100): Time resolved probabilities for absorption $P_{abs}(t)$ (a) and reflection $P_{ref}(t)$ (b) for different propagation methods: QM(2D) (pRS-2D rigid surface model, wave packet method), QM(3D) (p1SO-3D non rigid surface model, wave packet method), QCMD(V) (p1SO-3D non rigid surface model, QCMD with "exact" EMT potential), QCMD($\overline{V}$) (p1SO-3D non rigid surface model, QCMD with approximate, linearized EMT potential $\overline{V}$), TDSCF (p1SO-3D non rigid surface model, TDSCF with approximate EMT potential $\overline{V}$). The final time probabilities for the classical MD calculations for p1SO-3D are shown as horizontal, dot-dashed lines.

From Fig. 2.11(a) which gives $P_{v,ref}$ at the final propagation time at $t_f \approx 3$ ps, one notes that those parts of the wave packet which are reflected "create" none or only a few Cu oscillator quanta: $P_{v,ref}$ is essentially zero above $v = 15$ or so, and has a maximum at $v = 1$. In contrast, when H is absorbed there is a good chance that it leaves the surface oscillator in a highly excited vibrational state [Fig. 2.11(b)]: More than 50 quanta can be excited in the present example. This higher level of excitation is due to the fact that the absorbing species are longer in contact with the surface oscillator. One therefore expects that the H atoms absorbed in the bulk will eventually stick there. A significant part of the wave packet entering the surface region does not even reach the bulk, however, and sticks already in adsorption or subsurface bulk sites. We note further that the high level of vibrational excitation of the Cu oscillator is different from a more moderate energy transfer as observed, for example, during the dissociative adsorption of H_2 at metals [11] – simply because in the case of a single H much more kinetic energy is released. The strong coupling also makes the usefulness of certain approximate methods such as low-order perturbation theory, or the restriction to two-level environments questionable, even at zero surface temperature.

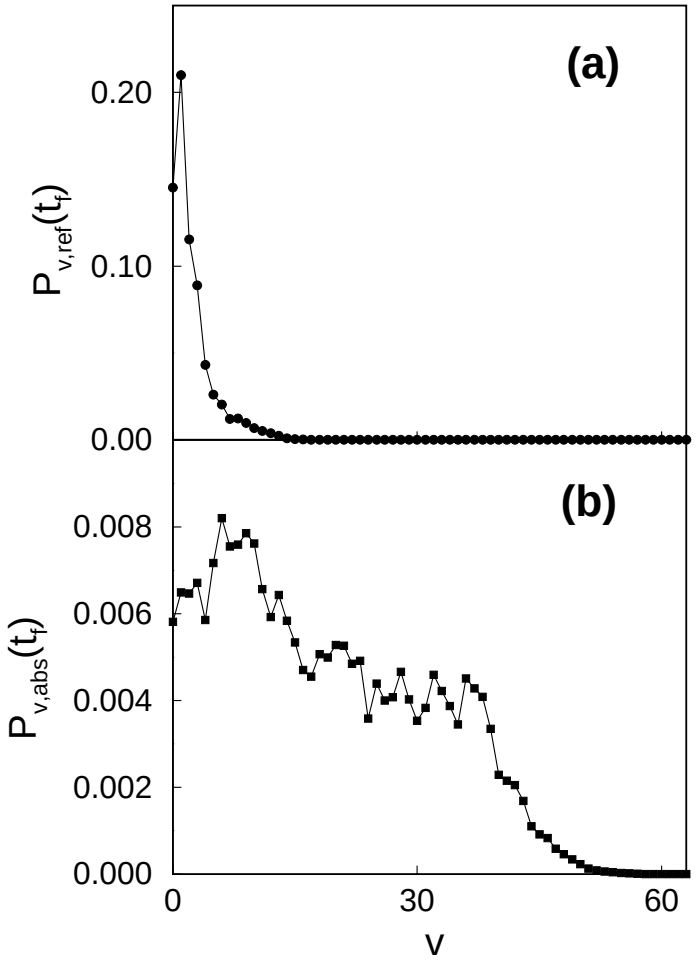

Figure 2.11: Single-oscillator (p1SO-3D) model: Cu oscillator state resolved final reflection (a) and absorption (b) probabilities, resulting from the "exact" QM calculation. Note that more than 50 vibrational quanta are excited in the surface oscillator in (b).

III. Single-oscillator case: "Approximate" calculations

In Fig. 2.10 and Table 2.5, also results from the approximate quantum methods [quantum-classical QCMD with exact (QCMD(V)), or approximate potentials (QCMD($\overline{V}$)), and TDSCF], are shown. The performance of these is as follows:

1. All approximate quantum methods get the main effects due to a non rigid surface qualitatively right, *i.e.*, the reflection probability is diminished at the expense of bulk or subsurface absorption, and adsorption.

2. All the methods fail quantitatively by grossly underestimating the extent of coupling between adsorbate and substrate. As a consequence, (i) $P_{ref}(t)$ for example, rises too quickly and saturates too early in comparison to the "exact" 3D SO reference [see Fig. 2.10(b)], (ii) the shift in the final reaction probabilities is too small. In particular, the approximate quantum methods predict almost negligible sticking in subsurface or adsorption sites – see Table 2.5. In summary, the approximate methods give results closer to the rigid surface one than to the exact reference.

3. The use of the approximate potential $\overline{V}$ (2.21) rather than the exact EMT potential (2.2) in the QCMD calculations does not cause much error; this is good news in view of the faster algorithm due to the approximate potential. It also means that both the harmonic substrate and the linear (in the bath modes) coupling approximations work in the present case, despite quite many quanta of the quantum SO are excited [see Fig. 2.11(b)].

4. The QCMD method with the approximate potential $\overline{V}$ is identical to the TDSCF approach with the same potential. In fact this equivalency has been proven for potentials of the form (2.21), for which the harmonic quantum "bath" oscillator follows the classical trajectory (2.31) [37]. Of course for more general potentials (*e.g.*, anharmonic ones),

TDSCF and QCMD are no longer equivalent and rather than using (2.31), 3N one dimensional Schrödinger equations must be solved for the "bath". Owing to the similarity of the QCMD(V) results to those derived from the simplified potential, here a more sophisticated TDSCF scheme for H/Cu(100) is not implemented. Note that the small remaining differences between the TDSCF and the QCMD($\overline{V}$) methods reported in Table 2.5 are due to the different numerical algorithms used – their magnitude therefore serves as an internal check for the accuracy of these algorithms (see section 2.3.5).

When looking at the final, classical MD results shown as horizontal lines in Fig. 2.10 (see also Table 2.5), one can clearly see that MD agrees better with the exact p1SO-3D quantum calculation than with the mean-field quantum ones. It is clear from Table 2.5 that not only are the final reflection and bulk absorption probabilities in better agreement, but also the classical subsurface absorption plus adsorption sticking probabilities are, at least when the "uncertain" trajectories which are still in the interaction region after 3 ps are tentatively counted as sticked. Hence, classical dynamics seems to perform better in this case than approximate quantum dynamics.

Although TDSCF (or the related QCMD) calculations have been shown to fail badly in certain cases [37, 61], there are other examples (including gas-surface ones), where these schemes perform remarkably well [62]. To understand the inaccuracy of these approximate quantum methods in the present application, one can assume that among the two basic assumptions underlying QCMD, namely (i) the single configuration ansatz for the total wave function and (ii) the classical approximation for a part of the system, only (i) is expected to be seriously wrong. The classical treatment of the heavy Cu atoms should be valid in view of the small ratio m/M. (In the QCMD schemes, the error introduced by the "Born-Oppenheimer"-type treatment of "fast" and "slow" modes, is of the order of $\mathcal{O}(\sqrt{m/M})$ [54].) In fact, the relatively better agreement between the fully classical and the exact quantum calculation indicates that even the H atoms do not behave very

quantum mechanically at these large impact energies. While the (partial) classical treatment seems therefore rather uncritical, the real problem arises from the single configuration ansatz.

To illustrate this, let us consider an initial 2D wave packet which is localized and Gaussian both in z_H and in x_H, approaching a movable Cu(100) surface. The latter is treated classically and Ehrenfest coupled to the 2D H wave packet through the EMT potential. To avoid interference effects due to periodic boundaries, a larger unit cell is chosen with lattice constant $a' = 8a$. Fig. 2.12 shows what happens when this initially localized wave packet hits the surface: Shortly after the gas-surface encounter, it disintegrates into many fragments that correspond to reflected, adsorbed, and subsurface and bulk absorbed parts, respectively. It is clear that the coupling of such a highly fractal wave packet to the substrate cannot be described by a single configuration, and mean field type forces must be incorrect. Therefore, though the TDSCF and hence the QCMD methods may be good when the wave packet is still far away from the surface, it must fail after the impact. Since the reaction probabilities one is interested in develop obviously only on the ps-timescale, the short-time accuracy of the TDSCF/QCMD methods known from the literature [63] is not sufficient to arrive at reasonable, final-time results in the present context. This is different from other reactions such as the dissociation of H_2 at surfaces which proceed within a few tenths of fs – in this case a QCMD approach proved in fact to be quite accurate [62].

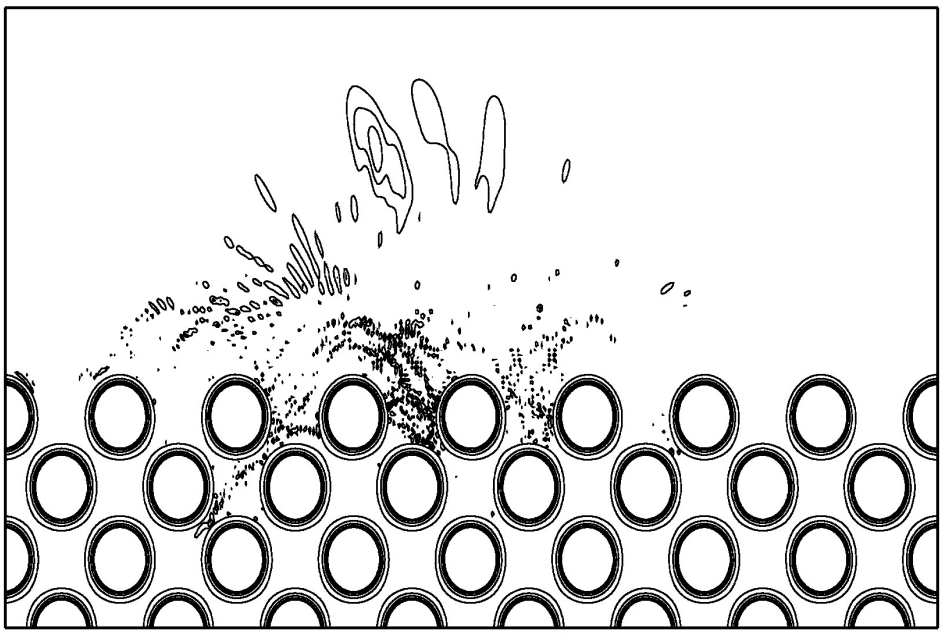

Figure 2.12: Snapshot after 8000 $\hbar/E_h$ propagation time of a 2D QCMD($\overline{V}$) Gaussian wave packet, initially localized in both x_H and z_H, and approaching a classical, moving Cu(100) surface. Shown are contours (at 0.00025 0.0002 0.00015 0.0001, and 0.00001 a_0^{-2}) of $|\psi(x_H, z_H, t)|^2$ shortly after impact on the surface. The initial WP is centered at $x_0 = 28.82\ a_0$ (corresponding to a displacement from the middle Cu atom in the top layer, of 1.5 a_0), and $z_0 = 17\ a_0$. It moves towards 5 movable Cu layers consisting of 8 Cu atoms each, with an initial average momentum of $(k_{0x}, k_{0z}) = (0, 5.20\ \hbar/a_0)$, corresponding to $E_{kin}(0) = 0.20$ eV. The width of the initial WP is $(\Delta x, \Delta z) = (0.961a_0, 0.961a_0)$.

2.4.2 Multiple-oscillator and other calculations

Though the single-configuration methods perform somewhat poor in the examples above, one should not completely give up on them. They serve as important starting points for more sophisticated approaches and are known to improve the higher dimensional the problem is [64], and / or at higher temperatures [57]. Even at cold surfaces and in low dimensional models qualitative trends are expected to be meaningful.

I. Multiple-oscillator calculations

To exploit the latter fact, various mean-field type quantum approaches were tested for the planar model in which five Cu layers were allowed to move (p5SO-7D), for the same four kinetic energies studied in Table 2.5. (The final propagation times, however, were always taken as $t_f = 125000\ \hbar/\mathrm{E}_h$.) In this case an "exact", fully quantum mechanical reference is not available. The final reaction probabilities for normal incidence are listed in Table 2.6. Fig. 2.13 gives the time evolution of these probabilities.

By comparing the results for a given propagation method for the lowest initial kinetic energy of $E_{kin}(0) = 0.00745$ E_h (0.20 eV) in Table 2.5 (single-oscillator case) to those in Table 2.6 (multiple-oscillator case), one sees that the more Cu layers move, the higher becomes the percentage of bulk absorbed H at the expense of a reduced reflection probability. Comparing the QCMD results (exact EMT potential), for the 5-oscillator case to those of the single-oscillator situation and to the rigid surface result, one finds P_{abs}(rigid)$\approx$ 0.16, P_{abs}(p1SO-3D, QCMD)$\approx$ 0.18, P_{abs}(p5SO-7D, QCMD)$\approx$ 0.22. This indicates that when including only one rather than five Cu oscillators less than half of the effect of the moving surface is captured, *i.e.*, it is not sufficient to include only one vibrating surface layer. (Test calculations reveal, however, that five moving layers are enough to converge those quantities which are of interest here.)

Method	$E_{kin}(0)/[E_h]$	P_{abs}	P_{ref}	P_{ads}	P_{sub}
QCMD(V)	0.00745	0.2173	0.7804	$2.1\ 10^{-3}$	$1.9\ 10^{-4}$
	0.01164	0.1794	0.8200	$4.9\ 10^{-4}$	$4.3\ 10^{-5}$
	0.01675	0.1657	0.8344	$4.5\ 10^{-5}$	$3.8\ 10^{-6}$
	0.02281	0.1280	0.8720	$1.5\ 10^{-5}$	$1.1\ 10^{-6}$
QCMD($\overline{V}$)	0.00745	0.2115	0.7790	0.008895	0.0006
	0.01164	0.1951	0.8037	0.00107	4.910^{-5}
	0.01675	0.1694	0.830	0.000378	3.010^{-5}
	0.02281	0.1425	0.8574	3.910^{-5}	2.5810^{-6}
TDSCF	0.00745	0.2115	0.7790	0.00885	0.0006
	0.01164	0.1948	0.8040	0.00107	2.210^{-5}
	0.01675	0.1689	0.8306	0.00037	1.810^{-5}
	0.02281	0.1424	0.8576	3.9810^{-5}	2.210^{-6}
	$E_{kin}(0)/[E_h]$	P_{abs}	P_{ref}	$P_{ads} + P_{sub}$	UC
MD	0.00745	0.3981	0.3560	0.1960	0.04986
	0.01164	0.3616	0.4533	0.1512	0.03391
	0.01675	0.3116	0.5402	0.1188	0.02940
	0.02281	0.2661	0.6167	0.0995	0.01770

Table 2.6: Multiple-oscillator p5SO-7D model: Comparison of different mean-field propagation methods with classical MD. Given are the final reaction probabilities ($t_f = 1250000\ \hbar/E_h$), for those four initial kinetic energies of the H wave packet considered in Table 2.4. The abbreviations are explained in the text.

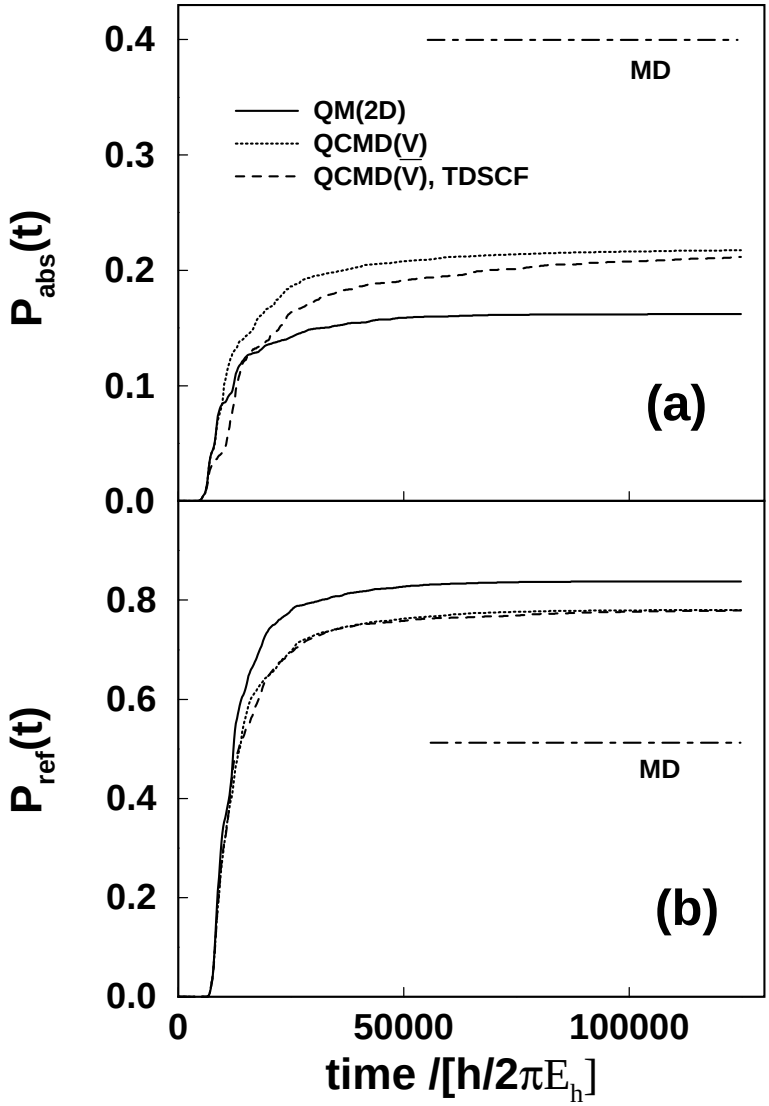

Figure 2.13: Rigid surface (pRS-3D) and multiple-oscillator (p5SO-7D) models for H/Cu(100): Time resolved probabilities for absorption $P_{abs}(t)$ (a) and reflection $P_{ref}(t)$ (b) for different propagation methods. See the caption of Fig. 2.10 for notation.

Qualitatively the same results are obtained from classical MD calculations. These, however, predict an even more pronounced role of deeper Cu layers – the absorption probability increases by almost a factor of 2 when changing from the single- to the multiple-oscillator model. The MD simulation further predicts that the sticking of H in subsurface or adsorption sites increases substantially as soon as more substrate degrees of freedom can be excited. Again for the lowest kinetic energy the sum of the probabilities to find H with "certainty" or with some "uncertainty", in the adsorption / subsurface regions increases from ≈ 0.09 in the single-oscillator model, to ≈ 0.25 in the multiple-oscillator model. This enhanced sticking probability is to be expected for a "softer" surface. Unfortunately, the mean-field quantum schemes again grossly underestimate the sticking probability, at least if one accepts that the classical calculation is the more accurate one in this case.

Both the single-configuration TDSCF-like schemes, and classical MD agree qualitatively in the trend predicted for higher kinetic energies of the projectiles. In the multiple-oscillator case, the absorption probability goes monotonically down when $E_{kin}(0)$ increases from 0.00745 to 0.02281 E_h, while P_{ref} goes up. This is in accord with the rigid surface result (Table 2.4), where however the behavior was not quite monotonic. (This is probably due to scattering resonances; these are "washed out" when the surface moves.) Again, at even higher $E_{kin}(0)$ one expects that the absorption probability should increase, for reasons similar to those discussed above.

Considering trends due to increasing projectile energies on the sticking in subsurface absorption and adsorption sites, we only refer to MD calculations since the mean-field sticking probabilities are unreliable here. From Table 2.6 one sees that the faster H atoms give not only less bulk absorption, but also less sticking. Closer inspection reveals that the falloff in both properties with $E_{kin}(0)$ runs approximately in parallel, hence both contribute about equally to an increasing reflection probability. These trends can again be rationalized with steering arguments, and with the fact that a faster projectile has less time to transfer energy to the moving surface and therefore to stick.

II. Other calculations: Non normal incidence and motion in 3 spatial directions

A few other calculations were carried out with the aim to test the performance of various methods, but also to gain additional insight in the scattering process.

Firstly, the above observations and conclusions concerning the methods hold true also for non-perpendicular impact for the H atom, *i.e.*, when one chooses $k_{0x} \neq 0$ in Eq. (2.11). Some "physical consequences" of non-normal impact are as follows. For the rigid surface case (pRS-2D) one finds that at non-normal incidence the absorption probability P_{abs} for a given impact energy usually increases, while the reflection probability P_{ref} decreases; at $0^o, E_{kin}(0) = 0.0074\ E_h$, exact quantum treatment: $P_{abs} \approx 0.16, P_{ref} \approx 0.84$ (Table 2.4), but at 45^o: $P_{abs} \approx 0.29$, $P_{ref} \approx 0.71$. The enhanced absorption probability at non-normal impact is due to the low-energy paths for absorption for H atoms approaching under an angle, as demonstrated in Figure 2.2. In contrast for non rigid surfaces, non-normal incidence leads to smaller P_{abs} and larger P_{ref}, relative to the normal-impact case. The adsorption plus subsurface absorption probability is not very dependent on the impact angle. Within the p5SO-7D model, and with a fully classical treatment, it is found for $E_{kin}(0) = 0.0074\ E_h$ and an impact angle of 0^o: $P_{abs} \approx 0.40$, $P_{ref} \approx 0.36$, $P_{ads} + P_{sub} \approx 0.20$ (Table 2.6), but at 45^o: $P_{abs} \approx 0.33$, $P_{ref} \approx 0.46$, $P_{ads} + P_{sub} \approx 0.16$. One possible explanation of this more subtle finding is that the moving Cu atoms block temporarily the low-energy pathways to absorption (Figure 2.2).

Secondly, the QCMD method based on the approximate potential (2.21) was used for a fully three dimensional study, where a 3D H wave packet approaches a Cu(100) surface consisting of classical, three dimensional oscillators. In this case one finds that the absorption probability increases at the expense of the reflection probability, when compared to the planar model. For example, a 3D wave packet with initial energy of ≈ 0.2 eV gives about one-half probability for both reflection and bulk absorption. (The adsorption

probability is again very small.) This trend is reasonable because a truly two dimensional Cu(100) surface is even more open than a 1D cut through it, and more absorption should therefore result. Again, no exact reference is available in this case and so it is also hard to say whether, and by how much the TDSCF-like methods improve in the higher dimensional model.

2.5 Conclusions

The conclusions which can be drawn from this chapter concern methodological and physical aspects. In terms of "physics" one can say that for systems like gas phase H approaching Cu(100), lattice phonons do matter despite of a large mass mismatch between the scatterers. The lattice vibrations lead to the sticking of H in subsurface and adsorption sites; still, bulk absorption and reflection dominate for this system. The large bulk absorption yields are due to both the "openness" of the Cu(100) surface and the "smallness" of the H atom – it will be much less pronounced for other atom/surface systems. In the case of H/Cu, there is non-negligible energy release when the atom approaches the surface; the accelerated atom crashes into the substrate, leading there to a considerable amount of excitation of the surface oscillator(s) which in turn influences the absorption and sticking dynamics. Still, the energy transfer between H and Cu is slow and therefore the H atom can travel as a "hot" atom for several ps and over long distances on the substrate before it finally absorbs or sticks. This is in accord with previous studies for H on metals [34, 49], but also for molecules such as CO [65]. However, a full quantitative account of these processes requires probably the inclusion of electronic friction which was neglected here. For the purely mechanical problem one finds that the "softer" the surface is made, the larger become the absorption and sticking yields at the expense of reflection. Reflection becomes more probable again when higher-energy H atoms approach the surface, which is due to a combination of dynamical steering, and energy transfer effects.

On the methodological side the biggest surprise was how bad the mean-field approaches perform for quantitative predictions, while classical mechanics performs rather well. In fact, for the present application the QCMD and TDSCF approaches get the effects of a moving surface only qualitatively right, and can only account for systematic trends. However, there will also be situations where the adsorbate behaves more quantum mechanically and where even only approximate quantum methods are to be preferred over classical ones. Such situations may arise when the projectile is less ener-

getic and / or when tunneling is important. Also, if the reaction is fast the mean-field method is expected to work well. Finally, the TDSCF method has been shown to remarkably improve at higher temperatures [57]. All the calculations above were for a surface at zero temperature. Also tested was the method for a surface held at finite T. Preliminary results suggested that at $T = 100$ K the results are still very close to the TDSCF results at $T = 0$ K. However, the method may work better at higher temperatures for which work should be done in the future. In any case problems with simple mean-field type approaches for certain gas-surface are clearly visible. Therefore, alternative routes such as non-Markovian density matrix theory, semiclassical schemes [66], or path integral methods [67] are worth pursuing.

The methods employed or cited above are all of the time-dependent type, and therefore well-suited to directly obtain information on characteristic timescales and for extension to explicitly time-dependent problems. More traditional approaches to inelastic atom-surface phonon scattering are of the time-independent type, notably the Distorted Wave Born Approximation (DWBA) for single-phonon excitation [68, 69]. The single-phonon regime is clearly not met by H/Cu (see Fig. 2.11), but a multi-phonon extension of the theory using a distorted wave Exponentiated Born Approximation (EBA) [70, 71, 72], would be interesting to compare with.